The quasiparticle band structure of zincblende and rocksalt ZnO

H Dixit, R Saniz, D Lamoen and B Partoens

CMT-group and EMAT, Departement Fysica, Universiteit Antwerpen, Groenenborgerlaan 171, B-2020 Antwerpen, Belgium

E-mail: Hemant.Dixit@ua.ac.be, Rolando.Saniz@ua.ac.be, Dirk.Lamoen@ua.ac.be and Bart.Partoens@ua.ac.be

Abstract
We present the quasiparticle band structure of ZnO in its zincblende (ZB) and rocksalt (RS) phases at the Γ point, calculated within the GW approximation. The effect of the p–d hybridization on the quasiparticle corrections to the band gap is discussed. We compare three systems, ZB-ZnO which shows strong p–d hybridization and has a direct band gap, RS-ZnO which is also hybridized but includes inversion symmetry and therefore has an indirect band gap, and ZB-ZnS which shows a weaker hybridization due to a change of the chemical species from oxygen to sulfur. The quasiparticle corrections are calculated with different numbers of valence electrons in the Zn pseudopotential. We find that the Zn^{20+} pseudopotential is essential for the adequate treatment of the exchange interaction in the self-energy. The calculated GW band gaps are 2.47 eV and 4.27 eV respectively, for the ZB and RS phases. The ZB-ZnO band gap is underestimated compared to the experimental value of 3.27 by ~0.8 eV. The RS-ZnO band gap compares well with the experimental value of 4.5 eV. The underestimation for ZB-ZnO is correlated with the strong p–d hybridization. The GW band gap for ZnS is 3.57 eV, compared to the experimental value of 3.8 eV.

(Some figures in this article are in colour only in the electronic version)

1. Introduction

The wide band gap semiconductor zinc oxide (ZnO) is an important material in optoelectronic device technology and is used in a number of applications such as visual displays, solar cells and so on. *Ab initio* first-principles calculations of ZnO are highly desired for designing new devices cost effectively. Although the ground state of ZnO has the wurtzite (WZ) structure, the metastable zincblende (ZB) and high pressure rocksalt (RS) phases have growing experimental interest [1, 2]. The zincblende phase of ZnO can be grown using molecular beam epitaxy. The zincblende phase may solve the challenge of controlling p-type conductivity in the optoelectronic devices [1].

The electronic structures of rocksalt and zincblende ZnO have been discussed [3] within the framework of density functional theory (DFT) [4, 5] using the local-density approximation (LDA). However, these calculations correctly describe the structural parameters rather than the optical properties. The reported electronic band structure shows a severe underestimation of the band gap. Since DFT, in principle, cannot describe electronic excitations, it is important to use the GW approximation [6], which gives a more realistic description of the band gap. The GW technique involves the ejection or injection of electrons that link the N-particle system with the $(N \pm 1)$-particle system. Thus, the GW approximation offers a strong physical basis for correlating the band energies obtained using Green's function with the experimental band gap. In this paper we present the GW band gaps, at the Γ point, calculated on top of the DFT band structure using the pseudopotential and the plane wave basis set.

In the case of II^B–VI semiconductor materials, it is important to include the localized 'd' orbitals in the cation pseudopotential (PP). The localized 'd' orbitals play an important role in bonding; hence their inclusion as valence orbital is essential for a correct structure [7]. However the DFT band structure, calculated using the pseudopotential with semicore 'd' states and the plane wave basis, shows serious underestimation of the band gap [3]. We further observe that the calculated quasiparticle band gap using the

GW approximation is also underestimated for ZnO. This observation is in agreement with the literature and is discussed below. Thus although use of the PP with semicore 'd' states yields the correct structure, it results in a poor quasiparticle correction questioning the validity of such a PP. We analyze this problem with a systematic study of the PP used and corresponding GW corrections to the band gap for the ZnO.

From the results published in the literature, we know that ZnO has proved to be a most challenging material for the GW approximation. The GW band gap is typically underestimated by LDA + *non-self-consistent GW* calculations. Indeed, the LDA PP with semicore 'd' states results in a *non-self-consistent GW* band gap of 1.36 eV [8] for ZB-ZnO compared to the experimental value of 3.27 eV. The all-electron *non-self-consistent GW* band gap for WZ-ZnO is 2.44 eV [9], which is smaller than the experimental value of 3.48 eV. Recently, the *self-consistent GW* scheme [10] and quasiparticle correction based on the generalized Kohn–Sham schemes [11, 8] have been used to improve the GW band gap for semiconductors and insulators. Also with the use of hybrid functionals in DFT [12, 13], a *non-self-consistent GW* band gap of 3.2 eV for WZ-ZnO is obtained. Although these schemes yield a closer estimate of the band gap within the GW approximation for ZnO, there is still a need for a parameter free theory. This is still a topic of current research. Our systematic study with PPs and hybridization can provide useful insight for future developments in this direction.

2. Theory

The GW approximation is based on the set of Hedin's equations that, when solved self-consistently, yield the exact interacting single-particle Green function [6]. In the GW approximation, the vertex corrections are neglected, resulting in a simplified self-energy operator, i.e.

$$\Sigma^{GW}(\mathbf{r}, \mathbf{r}'; \epsilon) = \frac{\mathrm{i}}{2\pi} \int \mathrm{d}\epsilon' \, \mathrm{e}^{(\mathrm{i}\epsilon'\delta)} \times G(\mathbf{r}, \mathbf{r}'; \epsilon + \epsilon') W(\mathbf{r}, \mathbf{r}'; \epsilon') \tag{1}$$

where δ is a positive infinitesimal number, and G and W are the electron Green function and dynamically screened Coulomb interaction, respectively. The quasiparticle equation

$$[T + V_{\mathrm{ext}}(\mathbf{r}) + V_{\mathrm{H}}(\mathbf{r})]\Psi_i(\mathbf{r}) + \int \mathrm{d}r' \, \Sigma(\mathbf{r}, \mathbf{r}'; \epsilon_i^{\mathrm{qp}})\Psi_i(\mathbf{r}')$$
$$= \epsilon_i^{\mathrm{qp}}\Psi_i(\mathbf{r}') \tag{2}$$

has then to be solved to obtain the quasiparticle energies ϵ_i^{qp} and the wavefunctions Ψ_i. In the above expression, T is the kinetic energy operator, and V_{ext} and V_{H} are the external potential and the Hartree potential, respectively. In practice, both the G and W operators are constructed within the quasiparticle approximation by using the Kohn–Sham wavefunctions Ψ_i and energies ϵ_i obtained from the DFT based calculations. In our work, the self-energy is calculated with the now well known *non-self-consistent GW* or single-step G_0W_0 approximation [6], where G_0 is the electron Green function corresponding to the DFT eigenvalues and eigenfunctions

$$G_0(\mathbf{r}, \mathbf{r}'; \epsilon) = \lim_{\delta \to 0^+} \Sigma_i \frac{\Psi_i(\mathbf{r})\Psi_i^*(\mathbf{r}')}{\epsilon - [\epsilon_i + \mathrm{i}\delta\,\mathrm{sgn}(E_{\mathrm{F}} - \epsilon_i)]} \tag{3}$$

and W_0 is the dynamically screened Coulomb interaction:

$$W_0(\mathbf{r}, \mathbf{r}'; \epsilon) = \int \mathrm{d}r'' \, \varepsilon^{-1}(\mathbf{r}, \mathbf{r}''; \epsilon)\nu(\mathbf{r}'', \mathbf{r}'). \tag{4}$$

Here E_{F} is the Fermi energy, ν is the bare Coulomb interaction and ε^{-1} is the inverse dielectric matrix. Hereafter we will refer to the G_0W_0 approximation used as the GW approximation for simplicity.

The DFT dielectric function (ε) is calculated in the random-phase approximation. Interpreting the DFT exchange–correlation potential V_{xc} as a frequency-independent, local approximation to the self-energy operator, the quasiparticle corrections to the DFT eigenvalues can be obtained from first-order perturbation theory with respect to $\Sigma - V_{\mathrm{xc}}$. This scheme has indeed been very successful in the study of a number of systems and properties [6, 8, 10].

3. Computational details

The electronic structure and the quasiparticle correction to the band gap at the Γ point have been calculated using the plane wave pseudopotential code ABINIT [18–20]. For the electronic structure the plane wave cutoff is chosen using the total energy convergence criterion of 2×10^{-2} eV. The atomic positions and structural parameters have been optimized by calculating the Hellmann–Feynman forces. The stresses are optimized with the criterion of 2×10^{-5} eV Å^{-3}. We choose a $4 \times 4 \times 4$ Monkhorst–Pack [21] k-point mesh which yields 10 k points in the irreducible Brillouin zone.

All PPs used are generated with the OPIUM [22] code according to the Troullier–Martins [23] method with Perdew–Zunger LDA [24]. The electronic configuration of the zinc atom is [Ne]$3s^2 3p^6 3d^{10} 4s^2$. The standard DFT PP treats the 3d and 4s electrons as valence ones and results in the Zn^{12+} PP. In this work we construct the Zn PP with 2, 12, 18 and 20 valence electrons. To generate the 20-electron PP (Zn^{20+} PP), a radius cutoff of 0.42 Å for 3s, 3p and 3d is chosen. It should be noted that we do not construct our 20-electron pseudopotential for the neutral zinc atom, but rather for the Zn ion with the 4s state unoccupied. This radius cutoff shows the smallest transferability error for ionic configurations of Zn (neutral, +1 and +2), at the cost of an increased plane wave cutoff. We have used 135 Ha (hartrees) as the energy cutoff for plane waves, when the Zn^{20+} PP is used. The radial cutoffs used in the construction of 2-, 12- and 18-electron PPs are 1.05 Å, 0.42 Å and 0.42 Å for 4s, 3p and 3d states respectively. We use the plane wave cutoff 30, 60 and 95 Ha for 2-, 12- and 18-electron PP respectively. The PP becomes harder with the inclusion of localized core orbitals in the valence.

The parameters used within ABINIT to calculate the self-energy are optimized with the convergence criterion of 0.01 eV for the band gap at Γ. We have found that, for both the screening and the self-energy calculation, 300 bands are sufficient to converge the GW band gap. The dielectric matrix is calculated with the plasmon-pole model [6] and is used to calculate the screening. We also calculate the dielectric matrix explicitly with 20 points along the real part and 4 points along the imaginary part of the frequency axis, avoiding the use of the
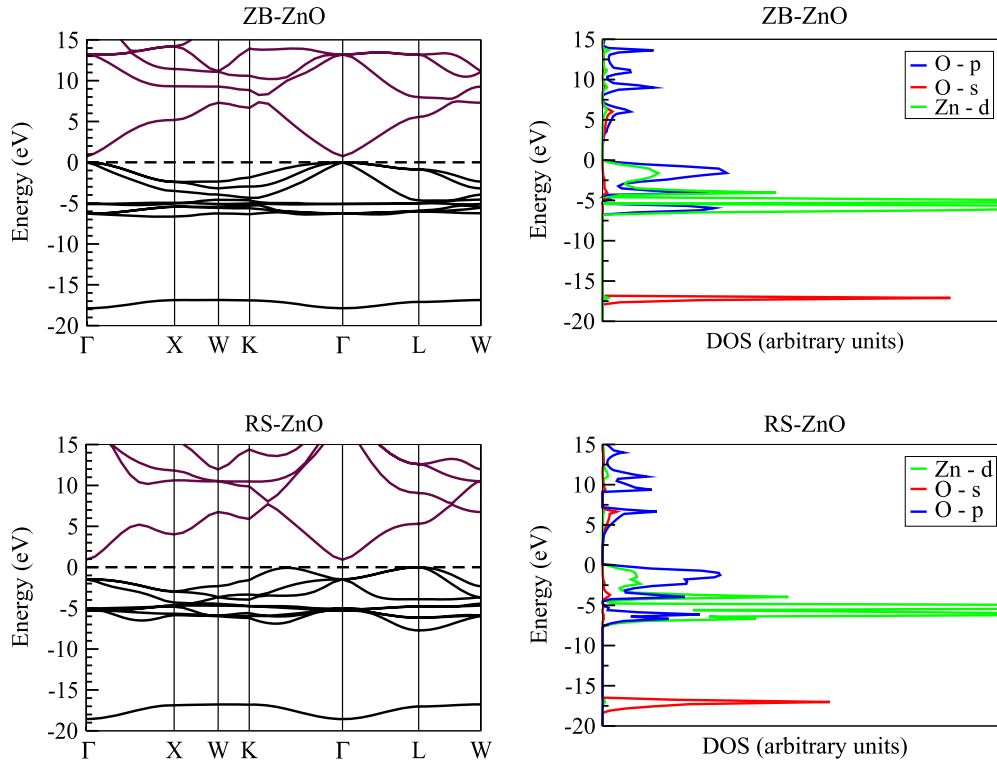
Figure 1. Band structure and projected density of states of the ZB and RS-ZnO (with the 12-electron Zn PP).

Table 1. Optimized lattice constants of ZnO and ZnS.

Structure	Lattice constant (theoretical) Å	Lattice constant (experiment) Å
ZB-ZnO	4.53	4.47[a]
RS-ZnO	4.25	4.28
ZB-ZnS	5.33	5.42

[a] The experimental lattice constant is smaller than the theoretical value due to the strain kinetics and lattice mismatch involved in growing ZB-ZnO films [1].

plasmon-pole model. We observe that the difference between the GW band gaps obtained with and without the plasmon-pole model is less than 0.05 eV. Hence we report the GW band gaps calculated using the plasmon-pole model.

4. Result and discussion

The optimized lattice constant, as listed in table 1, shows that the 12-electron PP accurately describes the structural parameters of ZnO and ZnS.

The calculated DFT band structure and projected density of states (PDOS) for the zincblende and the rocksalt structure are shown in figure 1. The PP used involves the 3d and 4s states in the valence of zinc. The DFT band structure shows that the upper part of the valence band of ZnO consists of extended Zn 3d and O 2p orbitals. The projected density of states clearly shows significant p–d (O 2p and Zn 3d) hybridization in the range of 0 to −6 eV. To get more insight into the p–d hybridization we have listed the projected weights of the Kohn–Sham wavefunctions at the Γ, K and L points and this list can be found as an appendix. The Zn 3d derived bands are split into two groups which are triply and doubly degenerate at Γ. The upper (doubly degenerate) band around −4.9 eV shows strong 'd' character while the lower (triply degenerate) band around −6.2 eV is hybridized with O p. The semicore 'd' states of Zn have a relatively high energy in the band structure compared to the experimental value of −8.81 eV, measured for WZ-ZnO [14]. Up to now there has been no experimental measurement of the 'd' energy levels for ZB-ZnO and RS-ZnO. However, we believe that the result for WZ-ZnO is also relevant for ZB-ZnO, as the two electronic band structures are very similar [3]. ZB-ZnO has a calculated direct band gap of 0.79 eV while RS-ZnO shows an indirect gap of 1.16 eV and the direct gap at Γ of 2.54 eV.

The nature of the band gap changes from direct to indirect going from the zincblende to the rocksalt phase. This change can be understood on the basis of the symmetry dependence of the interaction between anion 'p' states and cation 'd' states. In the ZB structure, the point group (T_d) does not contain an inversion center; thus the anion 'p' states and cation 'd' states can mix at any point in the Brillouin zone, because there are always 'p' or 'd' states belonging to the same representation [25]. This p–d interaction results in a fairly uniform upward shift of the upper valence bands. On the other hand the point group (O_h) of the RS structure contains an inversion center at the Γ point. The 'p' and 'd' states belong to a different representation at the Γ point in the RS structure and do not mix. At other points with lower symmetry,
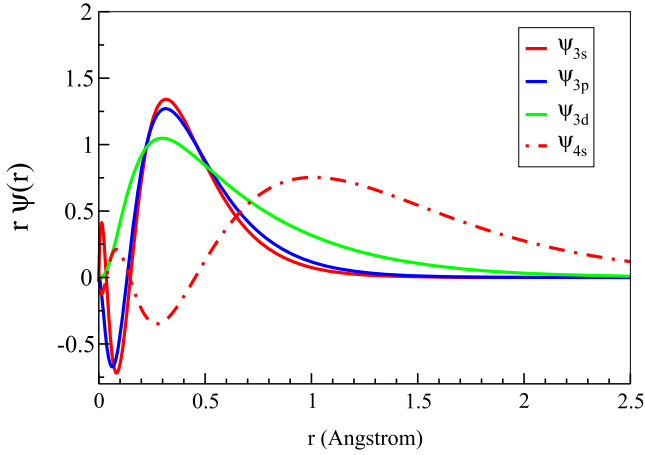
Figure 2. All-electron wavefunction plot for the Zn atom.

Table 2. The DFT-LDA and GW band gap (E_g) at Γ and the Zn d energy (E_d) level with the Zn^{12+} PP (all in eV) calculated at the optimized lattice constant.

Structure	E_g^{LDA}	E_g^{LDA+GW}	E_d^{LDA}	E_d^{LDA+GW}	E_d^{Exp}	E_{gap}^{Exp}
ZB-ZnO	0.79	**1.00**	−5.68	−4.57	−8.81	3.27
RS-ZnO	2.54	**3.72**				4.5

Table 3. The DFT-LDA and GW band gap and the Zn d energy (all in eV) at Γ, with four different pseudopotentials for ZB-ZnO (at experimental lattice constant(4.47 Å)).

Zn PP	E_g^{LDA}	E_g^{LDA+GW}	E_d^{LDA}	E_d^{LDA+GW}	Optimized lattice con. (Å)
Zn^{2+}	3.10	5.26	—	—	3.27
Zn^{12+}	0.83	1.09	−5.96	−4.90	4.53
Zn^{18+}	0.66	1.57	−6.36	−6.83	4.71
Zn^{20+}	0.88	2.53	−5.67	−6.53	4.50

the 'p' and 'd' states can mix in the Brillouin zone. The p–d interaction depends on the electron wavevector and the resulting p–d repulsion leads to an upward dispersion of the top valence bands in the Γ–K and Γ–L directions of the Brillouin zone. At the Γ point, five valence bands show a strong 'd' character and the top three valence bands have a strong 'p' character (see the appendix). However at the K and L points they mix with each other. The valence band maximum thus occurs away from the Γ point and the RS-ZnO has an indirect band gap.

We calculate the quasiparticle correction at the Γ point for ZB-and RS-ZnO with the Zn^{12+} PP for zinc. The quasiparticle band gaps and the Zn d energies, obtained with the Zn^{12+} PP, are shown in table 2. Such straightforward application of the GW approximation yields poor results for ZnO. The quasiparticle correction to the band gap for the RS-ZnO is approximately 1.2 eV whereas it results in a 0.2 eV shift for the ZB-ZnO. We also observe that the Zn 3d energy level in the quasiparticle band structure is shifted upwards compared to the DFT result and is away from the experimental value. This problem has been identified in the case of CdS by Rohlfing *et al* [16]; the unreasonable shift of the d energy levels is due to an inadequate treatment of the nonlinear exchange–correlation interaction in the self-energy. They have shown that when cation core states are successively included in the valence electron shell, the GW correction improves. The GW band gap is in excellent agreement with experiments for CdS, when Cd 4s, 4p, 4d and 5s states are used as valence in the PP. In case of ZnS a similar analysis holds and the GW band gap obtained is 3.5 eV, in close agreement to the experimental value of 3.8 eV [17]. We apply a similar study to ZB-and RS-ZnO along with ZnS which has a ZB structure. The change in the chemical environment, achieved by replacing oxygen with sulfur, leads to a weaker p–d hybridization between the anion and cation, which is discussed later.

The all-electron wavefunction plot for atomic Zn shows (figure 2) large spatial overlap of the 3s, 3p and 3d wavefunctions. Thus separating 3d orbitals from the core and therefore making an artificial division of 3d, 4s as valence is considered to be the cause of the poor quasiparticle

correction [16, 8]. The nonlinear exchange–correlation interaction, which depends on the spatial overlap of atomic orbitals, is not properly described in the self-energy when the Zn^{12+} PP is used. To analyze this fact we consider three different ionic Zn pseudopotentials with 2, 18 and 20 valence electrons respectively. The quasiparticle correction for the band gap and the Zn d energy are listed in table 3. The inclusion of 3p and 3s states in the valence description of the Zn atom results in the lowering of the Zn d energy and an improved quasiparticle correction for the band gap. The GW band gaps presented in this table are calculated at the experimental lattice constant of the ZB-ZnO to focus on the effect of the PP change, but the DFT lattice constants are listed in the last column. It should be noted that the experimental lattice constant used is less than the optimized lattice constant (due to film growth conditions); thus the corresponding DFT and GW band gaps are higher. The two-electron PP of Zn ($4s^2$) shows that the GW band gap overestimates the experimental value. Also the optimized lattice constant 3.27 Å, with this PP, is too small compared to the experimental value of 4.47 Å. Since the Zn d atomic energy lies in between the O s and O p atomic energy levels, the Zn d electrons play an important role in the bonding. Thus treating the 'd' electrons as core, thereby removing the p–d hybridization, leads to a GW gap that is too wide compared to experiment. The system is not screened enough in the absence of the 'd' electrons. For the 12-electron PP of Zn ($3d^{10}$, $4s^2$), the GW correction yields practically no shift. This is due to the fact that with the Zn^{12+} PP, the exchange energy contribution due to spatial overlap of '3d' with the '3p' and '3s' orbitals is neglected in the self-energy. This is supported by Zn^{18+} PP, where the GW gap is opened further and the Zn 3d energy level is now realigned with the DFT-LDA energy. It should be noted that the DFT lattice constant obtained with the Zn^{18+} PP is larger than the experimental value. There is no physical reason to separate the '3p' orbital from '3s' and in the construction of PP and we have added the Zn^{18+} PP result for completeness. Finally we construct a 20-electron PP to describe the exchange interaction properly in the self-energy calculation. With the 20-electron
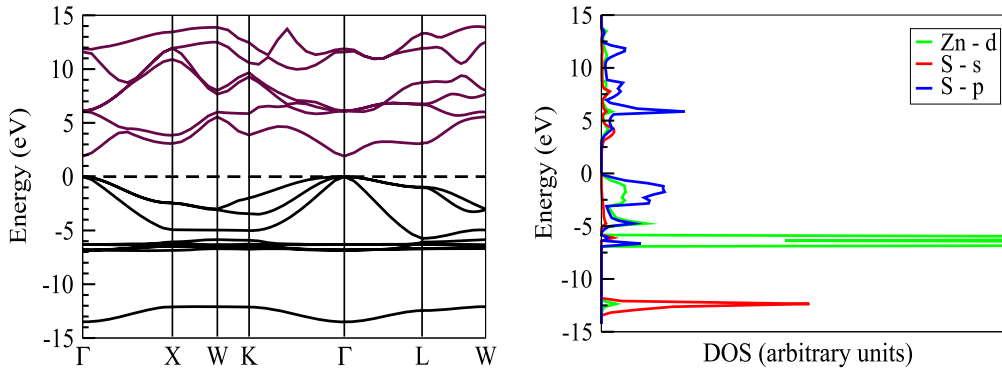
Figure 3. Band structure and projected density of states of ZnS (with the 12-electron Zn PP).

Table 4. Atomic orbital eigenvalues (in eV) for zinc, oxygen, and sulfur along with the energy difference between the anion p (ϵ_p^a) and cation d (ϵ_d^c) levels.

Zn 4s	−6.06	O 2s	−23.69	S 3s	−15.26
Zn 3d	−10.84	O 2p	−9.20	S 3p	−7.12
$\epsilon_p^a - \epsilon_d^c$			**1.64**		**3.72**

Table 5. The DFT-LDA and GW band gap and Zn d energy (all in eV) at Γ, for RS-ZnO and ZnS with four pseudopotentials (at the experimental lattice constant).

Zn PP	E_g^{LDA}	E_g^{LDA+GW}	E_d^{LDA}	E_d^{LDA+GW}	Optimized lattice con.
		RS-ZnO			Exp. lattice con. = 4.28 Å
Zn^{2+}	2.66	4.26	—	—	2.85
Zn^{12+}	2.38	3.52	−4.07	−1.74	4.25
Zn^{18+}	2.05	2.94	−4.71	−5.40	4.39
Zn^{20+}	2.39	3.77	−3.78	−5.21	4.21
		ZnS			Exp. lattice con. = 5.42 Å
Zn^{2+}	2.60	4.01	—	—	4.68
Zn^{12+}	1.87	2.64	−6.63	−4.30	5.33
Zn^{18+}	1.70	2.71	−7.27	−7.47	5.60
Zn^{20+}	1.77	3.38	−6.56	−7.16	5.32

PP, the Zn 3d energy level is positioned around −6.53 eV, about 1 eV lower than the DFT-LDA result, and is now closer to the experimental value. The calculated GW band gap is 2.53 eV, which is still lower by ∼0.8 eV than the experimental value (3.27 eV). However, this compares well with the all-electron result, 2.44 eV, for the WZ-ZnO [9]. Also the DFT optimized lattice constant with the 20-electron PP is in agreement with the experiment.

The underestimation of the GW band gap in ZB-ZnO, when the Zn^{20+} PP is used, can be attributed to the strong p–d hybridization between the anion and cation. To show this, we make a similar study for the RS-ZnO and ZnS. These two prototype systems are of interest because for RS-ZnO, the O p and the Zn d states do not mix at the Γ point. The five valence bands have strong Zn d character and the top three conduction bands have strong O p character and illustrate the absence of p–d mixing at the Γ. The change of chemical species from oxygen to sulfur shows a weaker p–d hybridization in the electronic structure of ZnS as can be seen from the band structure and PDOS in figure 3. The PDOS shows that the strongly dispersed valence bands in the energy range of 0 to −5 eV have a dominant S p character and the Zn d energy is located around −6.5 eV. The atomic orbital energies for zinc, oxygen and sulfur, calculated within the LDA using the OPIUM code, are listed in table 4. The p–d energy difference for ZnO is 1.64 eV compared to 3.72 eV for ZnS. Hence the electronic structure of ZnS shows a weaker hybridization compared to that of ZB-ZnO.

We now calculate the quasiparticle correction with the same set of PPs for RS-ZnO and ZnS. Table 5 lists the quasiparticle corrections and position of Zn 3d states. All the calculations are again done at the fixed value of the experimental lattice constant for a meaningful comparison of the band gap and Zn 3d level. We observe a similar trend for RS-ZnO and ZnS. The Zn^{2+} PP overestimates the GW

band gap. The Zn^{12+} PP gives an insufficient quasiparticle correction due to inadequate treatment of the exchange interaction in the self-energy. With the inclusion of 3p and 3s orbitals, the exchange interaction is now properly treated, which leads to lowering of the 'd' energy level compared to DFT-LDA result and opening of the GW band gap. This confirms the dependence of the self-energy on the spatial overlap of the atomic orbitals. Thus Zn^{20+} pseudopotential yields the best GW result.

Finally we calculate the GW band gap at the optimized lattice constant with the Zn^{20+} PP. The optimized lattice constants are 4.50, 4.21 and 5.32 Å for ZB-ZnO, RS-ZnO and ZnS respectively. These lattice constants are within an error of ∼1.5% compared to the experimental value. A schematic overview of the quasiparticle band structure is shown in figure 4. The Zn d energy level in the GW band structure is lower than the DFT-LDA counterpart for all of the systems. The GW band gap, at the Γ point, for ZB-ZnO is 2.47 eV compared to 3.27 eV from experiment. This band gap can be compared and is in agreement with the non-self-consistent GW band gap of 2.46 eV [26] and the all-electron result of 2.44 eV [9] for WZ-ZnO, as the two structures are similar.
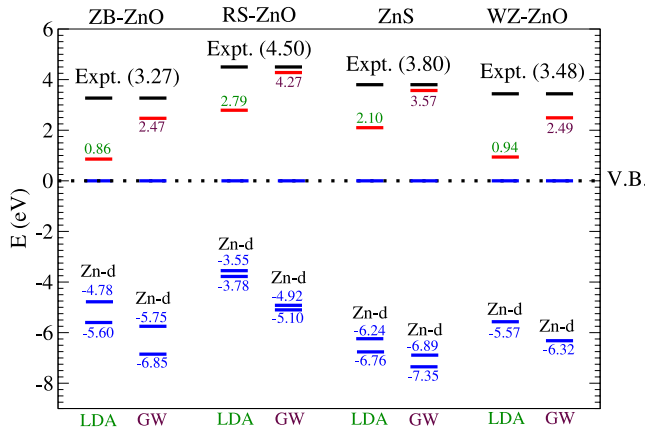
Figure 4. Schematic band structure showing the DFT-LDA and *GW* band gap along with position of the Zn d energies at the Γ point, calculated at the optimized lattice constant using 20-electron Zn PP.

For completeness, we have also obtained the *GW* gap of 2.49 eV for WZ-ZnO with this Zn^{20+} PP. The optimized lattice parameters for WZ-ZnO are $a = b = 3.192$ Å, $c = 5.162$ Å and $u = 0.380$, which compares well with the experimental values $a = b = 3.258$ Å, $c = 5.220$ Å and $u = 0.382$ [27]. For RS-ZnO we obtain a *GW* band gap of 4.27 eV, at the Γ point, compared to the experimental value of 4.5 eV. The *GW* band gap, at Γ, of ZnS is 3.57 eV which is in agreement with 3.54 eV published in the literature [15], and also compares with the experimental value of 3.8 eV. These results clearly show that the non-self-consistent *GW* correction depends on the extent of hybridization.

5. Conclusions

The systematic study of the PP and corresponding *GW* correction show that Zn^{20+} PP is essential for describing the localized d levels correctly in ZnO. The *GW* band gap obtained with Zn^{20+} PP is in agreement with the all-electron single-shot *GW* result [9, 26]. The ZB and RS phases of ZnO provide an interesting comparison between crystal symmetry and hybridization. The underestimation of the *GW* band gap in ZB-ZnO is correlated with the p–d overhybridization within the LDA. The RS phase includes the inversion symmetry at the Γ point in the Brillouin zone. The 'p' and 'd' states do not mix at the Γ point and therefore the *GW* correction at the Γ point is better for RS-ZnO compared to the ZB counterpart. Also the weakly hybridized system, ZnS, is well described with the Zn^{20+} PP and the *GW* approximation.

Acknowledgments

Appendix

We have listed the projected weights of the Kohn–Sham wavefunctions, for the three systems discussed, at the Γ, K and L points in tables A.1–A.3. The eleven bands presented include nine occupied (valence) and two unoccupied (conduction) bands. The ZB-ZnO is a strongly hybridized system—as the 'p' and 'd' states show significant mixing (table A.1). For the RS-ZnO, the p–d hybridization is absent at the Γ point (table A.2). The five valence bands (band index 2–6) show a strong 'd' character and the top three valence bands (band index 7–9) have a strong 'p' character. However at the K and L point they mix with each other. In the case of ZnS, the electronic structure shows a weaker hybridization compared to that of ZB-ZnO as is evident from the projected weights of the Kohn–Sham wavefunction at the Γ, K and L points, listed in table A.3.

Table A.1. The projected weights of the Kohn–Sham wavefunction at the LDA level for ZB-ZnO with the 12-electron Zn PP at the optimized lattice constant.

Band index	Zn 3d	Zn 4s	O s	O p	Energy (eV)
			At the Γ point		
1	0.00	0.00	0.88	0.00	−17.91
2	0.76	0.00	0.00	0.28	−6.19
3	0.76	0.00	0.00	0.28	−6.19
4	0.76	0.00	0.00	0.28	−6.19
5	0.98	0.00	0.00	0.02	−4.94
6	0.98	0.00	0.00	0.02	−4.94
7	0.28	0.00	0.00	0.69	0.00
8	0.28	0.00	0.00	0.69	0.00
9	0.28	0.00	0.00	0.69	0.00
10	0.00	0.30	0.30	0.00	0.79
11	0.00	0.00	0.00	0.00	13.40
			At the K point		
1	0.00	0.00	0.94	0.00	−16.88
2	0.55	0.05	0.00	0.36	−6.28
3	0.77	0.00	0.00	0.24	−5.51
4	0.87	0.01	0.00	0.10	−5.19
5	0.98	0.00	0.00	0.00	−4.87
6	0.15	0.15	0.00	0.58	−4.49
7	0.91	0.17	0.01	0.03	−4.35
8	0.40	0.03	0.00	0.42	−2.91
9	0.23	0.00	0.00	0.64	−1.84
10	0.12	0.00	0.04	0.10	6.68
11	0.01	0.43	0.03	0.28	8.86
			At the L point		
1	0.00	0.00	0.93	0.00	−17.10
2	0.07	0.15	0.00	0.59	−5.99
3	0.77	0.00	0.00	0.25	−5.94
4	0.77	0.00	0.00	0.25	−5.94
5	0.98	0.00	0.00	0.00	−4.86
6	0.98	0.00	0.00	0.00	−4.85
7	0.87	0.03	0.01	0.08	−4.54
8	0.24	0.00	0.00	0.68	−0.86
9	0.24	0.00	0.00	0.68	−0.86
10	0.03	0.34	0.19	0.01	5.62
11	0.05	0.03	0.00	0.44	7.96

Table A.2. The projected weights of the Kohn–Sham wavefunction at the LDA level for RS-ZnO with the 12-electron Zn PP at the optimized lattice constant.

Band index	Zn 3d	Zn 4s	O s	O p	Energy (eV)
			At the Γ point		
1	0.00	0.00	0.86	0.00	−18.25
2	0.96	0.00	0.00	0.00	−5.38
3	0.96	0.00	0.00	0.00	−5.38
4	0.96	0.00	0.00	0.00	−5.38
5	0.98	0.00	0.00	0.00	−5.18
6	0.98	0.00	0.00	0.00	−5.18
7	0.00	0.00	0.00	0.96	−1.17
8	0.00	0.00	0.00	0.96	−1.17
9	0.00	0.00	0.00	0.96	−1.17
10	0.00	0.43	0.41	0.00	1.37
11	0.40	0.00	0.00	0.00	18.36
			At the K point		
1	0.00	0.00	0.94	0.00	−16.52
2	0.60	0.04	0.00	0.28	−6.16
3	0.39	0.00	0.00	0.44	−5.86
4	0.78	0.00	0.00	0.22	−5.66
5	0.99	0.00	0.00	0.00	−4.92
6	0.87	0.01	0.02	0.08	−4.86
7	0.60	0.00	0.00	0.31	−3.92
8	0.45	0.10	0.01	0.38	−3.22
9	0.23	0.00	0.00	0.67	−1.41
10	0.00	0.57	0.05	0.10	6.43
11	0.11	0.02	0.04	0.25	10.09
			At the L point		
1	0.00	0.00	0.94	0.00	−16.69
2	0.29	0.19	0.00	0.48	−7.51
3	0.77	0.00	0.00	0.25	−6.21
4	0.77	0.00	0.00	0.25	−6.21
5	0.98	0.00	0.00	0.00	−4.96
6	0.98	0.00	0.00	0.00	−4.96
7	0.71	0.09	0.00	0.20	−3.92
8	0.28	0.00	0.00	0.71	0.11
9	0.28	0.00	0.00	0.71	0.11
10	0.00	0.00	0.21	0.01	5.55
11	0.00	0.36	0.00	0.55	9.44

Table A.3. The projected weights of the Kohn–Sham wavefunction at the LDA level for ZnS with the 12-electron Zn PP at the optimized lattice constant.

Band index	Zn 3d	Zn 4s	S s	S p	Energy (eV)
			At the Γ point		
1	0.00	0.00	0.69	0.00	−13.49
2	0.88	0.00	0.00	0.08	−6.82
3	0.88	0.00	0.00	0.08	−6.82
4	0.88	0.00	0.00	0.08	−6.82
5	0.97	0.00	0.00	0.00	−6.30
6	0.97	0.00	0.00	0.00	−6.30
7	0.14	0.00	0.00	0.70	0.00
8	0.14	0.00	0.00	0.70	0.00
9	0.14	0.00	0.00	0.70	0.00
10	0.00	0.29	0.30	0.00	1.90
11	0.25	0.00	0.00	0.38	6.10
			At the K point		
1	0.06	0.00	0.79	0.00	−12.11
2	0.80	0.01	0.00	0.09	−6.74
3	0.92	0.00	0.00	0.05	−6.53
4	0.94	0.01	0.00	0.01	−6.42
5	0.97	0.00	0.00	0.00	−6.26
6	0.91	0.00	0.03	0.00	−5.97
7	0.10	0.29	0.00	0.38	−4.97
8	0.10	0.00	0.00	0.46	−3.49
9	0.07	0.00	0.00	0.59	−1.73
10	0.06	0.10	0.03	0.04	3.86
11	0.03	0.17	0.00	0.28	5.86
			At the L point		
1	0.04	0.04	0.79	0.00	−12.44
2	0.89	0.00	0.00	0.06	−6.70
3	0.89	0.00	0.00	0.06	−6.70
4	0.97	0.00	0.00	0.00	−6.27
5	0.97	0.00	0.00	0.00	−6.27
6	0.90	0.00	0.02	0.00	−6.08
7	0.02	0.02	0.00	0.41	−5.73
8	0.10	0.00	0.00	0.65	−0.97
9	0.10	0.00	0.00	0.65	−0.97
10	0.01	0.30	0.19	0.03	3.07
11	0.04	0.00	0.00	0.27	6.73

References

[1] Ashrafi A and Jagadish C 2007 *J. Appl. Phys.* **102** 071101
[2] Sans J A, Segura A, Manjón F J, Marí B, Muñoz A and Herrera-Cabrera M J 2005 *Microelectron. J.* **36** 928
[3] Schleife A, Fuchs F, Furthmüller J and Bechstedt F 2006 *Phys. Rev. B* **73** 245212
[4] Hohenberg P and Kohn W 1964 *Phys. Rev.* **136** B684
[5] Kohn W and Sham L J 1965 *Phys. Rev.* **140** A1133
[6] Aulbur W G, Jönsson L and Wilkins J W 2000 *Solid State Phys.* **54** 1
[7] Schröer P, Krüger P and Pollmann J 1993 *Phys. Rev. B* **47** 6971
[8] Rinke P, Qteish A, Neugebauer J, Freysoldt C and Scheffler M 2005 *New J. Phys.* **7** 126
[9] Usuda M, Hamada N, Kotani T and van Schilfgaarde M 2002 *Phys. Rev. B* **66** 125101
[10] Shishkin M and Kresse G 2007 *Phys. Rev. B* **75** 235102
[11] Fuchs F, Furthmüller J, Bechstedt F, Shishkin M and Kresse G 2007 *Phys. Rev. B* **76** 115109
[12] King P D C *et al* 2009 *Phys. Rev. B* **79** 205205
[13] Preston A R H *et al* 2008 *Phys. Rev. B* **78** 155114
[14] Ley L, Pollak R A, McFeely F F, Kowalczyk S P and Shirley D A 1974 *Phys. Rev. B* **9** 600
[15] Miyake T, Zhang P, Cohen M L and Louie S G 2006 *Phys. Rev. B* **74** 245213
[16] Rohlfing M, Krüger P and Pollmann J 1995 *Phys. Rev. Lett.* **75** 3489
[17] Rohlfing M, Krüger P and Pollmann J 1998 *Phys. Rev. B* **57** 6485
[18] Gonze X *et al* 2002 *Comput. Mater. Sci.* **25** 478
[19] Gonze X *et al* 2005 *Z. Kristallogr.* **220** 558
[20] Bruneval F, Vast N and Reining L 2006 *Phys. Rev. B* **74** 045102
[21] Monkhorst H D and Pack J D 1976 *Phys. Rev. B* **13** 5188
[22] http://opium.sourceforge.net/index.html
[23] Troullier N and Martins J L 1991 *Phys. Rev. B* **43** 1993
[24] Perdew J P and Zunger A 1981 *Phys. Rev.* B **23** 5048
[25] Wei S-H and Zunger A 1988 *Phys. Rev. B* **37** 8958
[26] Kotani T, van Schilfgaarde M and Faleev S V 2007 *Phys. Rev. B* **76** 165106
[27] Decremps F, Datchi F, Saitta A M, Polian A, Pascarelli S, Di Cicco A, Itié J P and Baudelet F 2003 *Phys. Rev. B* **68** 104101